Tidal evolution of eccentric orbits in massive binary systems. A study of resonance locking

Witte, M.G.; Savonije, G.J.

Published in:
Astronomy & Astrophysics

A&A manuscript no.
(will be inserted by hand later)

Your thesaurus codes are:
06(02.08.1; 08.02.1; 08.15.1; 08.18.1)

ASTRONOMY AND ASTROPHYSICS

October 2, 2006

The dynamical tide in a rotating 10 $\mathrm{M}_\odot$ main sequence star

a study of g- and r-mode resonances

M.G. Witte[⋆] **and G.J. Savonije**[⋆⋆]

Astronomical Institute 'Anton Pannekoek', University of Amsterdam, Kruislaan 403, 1098 SJ Amsterdam, The Netherlands

Received 19 July 1998 / Accepted ¡date¿

Abstract. We study the linear, but fully non-adiabatic tidal response of a uniformly rotating, somewhat evolved ($X_\mathrm{c} = 0.4$), 10 $\mathrm{M}_\odot$ main sequence star to the dominant $l = 2$ components of its binary companion's tidal potential. This is done numerically with a 2D implicit finite difference scheme. We assume the spin vector of the 10 $\mathrm{M}_\odot$ star to be aligned perpendicular to the orbital plane and calculate the frequency $\bar{\sigma}$ and width of the resonances with the prograde and retrograde gravity (g) modes as well as the resonances with quasi-toroidal rotational (r) modes for varying rotation rates Ω_s of the main sequence star. For all applied forcing frequencies we determine the rate of tidal energy and angular momentum exchange with the companion. In a rotating star tidal energy is transferred from $l = 2$ g-modes to g-modes of higher spherical degree ($l = 4, 6, 8, \ldots$) by the Coriolis force. These latter modes have shorter wavelength and are damped more heavily, so that the $l = 2$ resonant tidal interaction tends to be reduced for large rotation rates Ω_s. On the other hand, the density of potential resonances (a broad l spectrum) increases. We find several inertially excited unstable $l > 4$ g-modes, but not more than one (retrograde) unstable $l = 2$ g-mode and that only for rapid rotation. Our numerical results can be applied to study the tidal evolution of eccentric binaries containing early type B-star components.

Key words: Hydrodynamics– Stars: binaries: close– oscillations– rotation

1. Introduction

Zahn (1977) initiated the study of radiative damping of the dynamical tide as a viable mechanism for effective tidal interaction in early type close binary systems. Savonije & Papaloizou (1984) were the first to perform fully non-adiabatic calculations of the dynamical tide and to study the interplay between stellar- and tidal evolution which appears crucial in understanding the effects of tides in early type stars. More recently, Papaloizou & Savonije (1997) and Savonije & Papaloizou (1997) (from now on SP97) studied the effects of rotation on the dynamical tide. To this end a 2D implicit code was developed for which the effects of the Coriolis force on the non-radial oscillations are taken fully into account. These earlier studies of rotational effects were based on a chemically homogeneous 20 $\mathrm{M}_\odot$ star and were focussed on the low-frequency inertial regime, i.e. to forcing frequencies $\bar{\sigma} < 2\Omega_\mathrm{s}$, where $\bar{\sigma}$ is the forcing frequency in the frame corotating with the star at a rate Ω_s. The present study extends these calculations to a somewhat evolved (with core hydrogen abundance $X_\mathrm{c} = 0.4$) 10 $\mathrm{M}_\odot$ star whereby the forcing frequency $\bar{\sigma}$ runs from low (high radial order g-modes) to high frequencies (up to g_1). The motivation for this work is that we intend to apply the calculated energy and angular momentum exchange rates with the companion to study the tidal evolution of eccentric early type binary systems. Recently several new studies of tidal evolution in eccentric early type binaries (with a compact companion) have appeared (e.g. Kumar & Goodman 1996; Lai 1997). However, these studies have not considered the important effect of rotational (r) modes on the tidal exchange of angular momentum in eccentric binary systems. We anticipate interesting tidal effects in eccentric binaries by the counteracting effects of resonant prograde g-modes and retrograde r-modes when the early type component is rotating near its 'pseudo' synchronous rate at periastron. This will be studied in a following paper.

2. Basic equations

We consider a uniformly rotating, early type star with mass M_s and radius R_s in a close binary with circular orbit with angular velocity ω and orbital separation a. We assume the stellar angular velocity of rotation $\mathbf{\Omega}_\mathrm{s}$ to be much smaller than its break-up speed, i.e. $(\Omega_\mathrm{s}/\Omega_\mathrm{c})^2 \ll 1$, with $\Omega_\mathrm{c}^2 = GM_\mathrm{s}/R_\mathrm{s}^3$, so that effects of centrifugal distortion ($\propto \Omega_\mathrm{s}^2$) may be neglected in first approximation. We wish to study the response of this uniformly rotating star to a perturbing time-dependent tidal force. The Coriolis acceleration is proportional to Ω_s and we take its effect on the tidally induced motions in the star fully into account. We use spherical coordinates (r, ϑ, φ), with origin at the stellar centre, whereby $\vartheta = 0$ corresponds to its rotation axis which we assume to be parallel to the orbital angular momentum vector. We take the coordinates to be non-rotating.

⋆ marnix@astro.uva.nl
⋆⋆ gertjan@astro.uva.nl

As is well known, in a non-rotating star the solutions of the linearized non-radial stellar oscillation equations can be expressed in terms of spherical harmonics, i.e. the spatial part of each mode can be fully separated into r-, ϑ- and φ-factors (e.g. Ledoux & Walraven 1958) $U(r,\vartheta,\varphi) = u(r)\,P_l^m(\cos\vartheta)\,\mathrm{e}^{-\mathrm{i}m\varphi}$, where P_l^m represents the associated Legendre polynomials for l and m.

The introduction of the Coriolis force, however, destroys the full separability of the oscillation equations, it only being retained for the φ-dependence. It turns out (e.g. Berthomieu et al. 1978) that two independent sets of approximately spheroidal oscillation modes exist: modes in which the density perturbation is *even* with respect to reflection in the equatorial plane, which have $l-|m|$ even valued, and modes with *odd* symmetry for the density, having $l-|m|$ odd valued. In addition, for each l, there is a set of quasi-toroidal r-modes (e.g. Papaloizou & Pringle 1978) which couple with the spheroidal modes of $l\pm1$.

Let us denote perturbed Eulerian quantities like pressure P', density ρ', temperature T' and energy flux $\boldsymbol{F}'$ with a prime. The linearized hydrodynamic equations governing the non-adiabatic response of the uniformly rotating star to the perturbing potential Φ_T may then be written

$$\left[\left(\frac{\partial}{\partial t}+\Omega_\mathrm{s}\frac{\partial}{\partial\varphi}\right)v_i\right]\hat{\boldsymbol{e}}_i+2\Omega_\mathrm{s}\boldsymbol{k}\times\boldsymbol{v}'$$

$$=-\frac{1}{\rho}\nabla P'+\frac{\rho'}{\rho^2}\nabla P-\nabla\Phi_\mathrm{T}, \tag{1}$$

$$\left(\frac{\partial}{\partial t}+\Omega_\mathrm{s}\frac{\partial}{\partial\varphi}\right)\rho'+\nabla\cdot(\rho\boldsymbol{v}')=0, \tag{2}$$

$$\left(\frac{\partial}{\partial t}+\Omega_\mathrm{s}\frac{\partial}{\partial\varphi}\right)[S'+\boldsymbol{v}'\cdot\nabla S]=-\frac{1}{\rho T}\nabla\cdot\boldsymbol{F}', \tag{3}$$

$$\frac{\boldsymbol{F}'}{F}=\left(\frac{\mathrm{d}T}{\mathrm{d}r}\right)^{-1}\left[\left(\frac{3T'}{T}-\frac{\rho'}{\rho}-\frac{\kappa'}{\kappa}\right)\nabla T+\nabla T'\right], \tag{4}$$

where $\hat{\boldsymbol{e}}_i$ are the unit vectors of our spherical coordinate system, $\boldsymbol{k}$ is the unit vector along the rotation axis, $\boldsymbol{v}'$ denotes the velocity perturbation, κ the opacity of stellar material and S its specific entropy. These perturbation equations represent, respectively, conservation of momentum, conservation of mass and conservation of energy, while the last equation describes the radiative diffusion of the perturbed energy flux. For simplicity we adopt the Cowling (1941) approximation, i.e. we neglect perturbations to the gravitational potential caused by the stellar distortion. We also neglect perturbations of the nuclear energy sources and of convection.

For a circular orbit (with orbital angular speed ω) the companion's perturbing potential can be expanded as the real part of (e.g. Morse & Feshbach 1952):

$$\Phi_\mathrm{T}(r,\vartheta,\varphi,t)=-\frac{GM_\mathrm{p}}{a}\sum_{l=0}^{\infty}\sum_{m=0}^{l}\epsilon_m\frac{(l-m)!}{(l+m)!}\left(\frac{r}{a}\right)^l$$

$$\cdot\,P_l^m(\cos\vartheta)\,P_l^m(\cos\frac{\pi}{2})\,\mathrm{e}^{\mathrm{i}m(\omega t-\varphi)} \tag{5}$$

where M_p is the companion's mass, a the orbital separation, $P_l^m(\cos\vartheta)$ the associated Legendre polynomial and $\epsilon_m=1$ for $m=0$ and 2 for $m>0$. We will consider only the dominant $l=2$ components of the tidal forcing. Adopting the same azimuthal m symmetry and time dependence for the perturbed quantities as the forcing potential, the perturbed velocity can be expressed as $\boldsymbol{v}'=\mathrm{i}\bar{\sigma}\boldsymbol{\xi}$, where $\bar{\sigma}=m(\omega-\Omega_\mathrm{s})$ is the forcing frequency felt by a mass element in the uniformly rotating star and $\boldsymbol{\xi}$ is the displacement vector.

The perturbations can be written as e.g. $\xi_r(r,\vartheta,\varphi,t)=\widehat{\xi_r}(r,\vartheta)\,\mathrm{e}^{\mathrm{i}m(\omega t-\varphi)}$ where ξ_r is the radial component of the displacement vector, while $\widehat{\xi_r}(r,\vartheta)$ is assumed complex to describe the azimuthal phase shift with respect to the forcing potential (5) induced by any occurring dissipation, e.g. turbulent viscosity or radiative damping, see energy equation below.

The current equations contain extra terms compared to those in SP97 because of the occurring mean-molecular weight (μ_a)-gradients near the edge of the convective core. We assume diffusive mixing to be negligible on the (oscillation) timescales under consideration, so that the Lagrangian variation of the mean molecular weight $\delta\mu_a=0$ or $\frac{\mu_a'}{\mu_a}=-\frac{\mathrm{d}\ln\mu_a}{\mathrm{d}r}\xi_r$. We can thus use

$$\frac{P'}{P}=\chi_\rho\left(\frac{\rho'}{\rho}\right)+\chi_T\left(\frac{T'}{T}\right)-\chi_\mu\frac{\mathrm{d}\ln\mu_a}{\mathrm{d}r}\xi_r \tag{6}$$

to eliminate the pressure perturbation, where $\chi_\rho=\frac{\partial\ln P}{\partial\ln\rho}$, $\chi_T=\frac{\partial\ln P}{\partial\ln T}$ and $\chi_\mu=\frac{\partial\ln P}{\partial\ln\mu_a}$ follow from the equation of state.

Writing for simplicity from now on ξ_r for $\widehat{\xi_r}(r,\vartheta)$, etc., while dividing out the factor $\mathrm{e}^{\mathrm{i}m(\omega t-\varphi)}$, Eqs. 1–4 yield the seven scalar Eqs. 7–13 given below.

First of all we write out the perturbed equation of continuity

$$\frac{\rho'}{\rho}=-\frac{1}{r^2\rho}\frac{\partial}{\partial r}\left(r^2\rho\xi_r\right)-\frac{1}{r\sin\vartheta}\frac{\partial}{\partial\vartheta}\left(\sin\vartheta\,\xi_\vartheta\right)+\frac{\mathrm{i}m}{r\sin\vartheta}\xi_\varphi. \tag{7}$$

We can use (7) to eliminate the term $\frac{\partial\xi_r}{\partial r}$ introduced by the radial derivative of the pressure perturbation (through (6)) from the radial equation of motion, so that the latter equation can be expressed (after adding viscous terms to introduce turbulent damping in convective regions, see SP97) as

$$\left[\rho\bar{\sigma}^2-\frac{P\chi_\mu}{\rho r^2}\frac{\mathrm{d}\ln\mu_a}{\mathrm{d}r}\frac{\mathrm{d}(\rho r^2)}{\mathrm{d}r}+P\frac{\mathrm{d}(\chi_\mu\frac{\mathrm{d}\ln\mu_a}{\mathrm{d}r})}{\mathrm{d}r}\right.$$

$$\left.+\chi_\mu\frac{\mathrm{d}P}{\mathrm{d}r}\frac{\mathrm{d}\ln\mu_a}{\mathrm{d}r}\right]\xi_r+\left[2\mathrm{i}\rho\bar{\sigma}\Omega_\mathrm{s}\sin\vartheta+\mathrm{i}m\frac{P\chi_\mu}{r\sin\vartheta}\frac{\mathrm{d}\ln\mu_a}{\mathrm{d}r}\right]\xi_\varphi$$

$$+\mathrm{i}\bar{\sigma}\frac{\rho\zeta}{r^2}\left[\left(1-\mu^2\right)\frac{\partial^2}{\partial\mu^2}\xi_r-2\mu\frac{\partial}{\partial\mu}\xi_r-\frac{4}{1-\mu^2}\xi_r\right]$$

$$+\frac{\mathrm{i}\bar{\sigma}}{r^2}\frac{\partial}{\partial r}\left(\rho\zeta r^2\frac{\partial\xi_r}{\partial r}\right)-\frac{P\chi_\mu}{r\sin\vartheta}\frac{\mathrm{d}\ln\mu_a}{\mathrm{d}r}\frac{\partial}{\partial\vartheta}(\sin\vartheta\,\xi_\vartheta)$$

$$+\left[\frac{\mathrm{d}P}{\mathrm{d}r}-P\chi_\mu\frac{\mathrm{d}\ln\mu_a}{\mathrm{d}r}-P\frac{\mathrm{d}\chi_\rho}{\mathrm{d}r}-\chi_\rho\frac{\mathrm{d}P}{\mathrm{d}r}\right]\left(\frac{\rho'}{\rho}\right)$$

$$-P\chi_\rho\frac{\partial}{\partial r}\left(\frac{\rho'}{\rho}\right)-\left[P\frac{\mathrm{d}\chi_T}{\mathrm{d}r}+\chi_T\frac{\mathrm{d}P}{\mathrm{d}r}\right]\left(\frac{T'}{T}\right)$$

$$-P\chi_T\frac{\partial}{\partial r}\left(\frac{T'}{T}\right)=-\rho\frac{\partial\Phi_\mathrm{T}}{\partial r} \tag{8}$$

where $\mu=\cos\vartheta$ and ζ is the coefficient of turbulent viscosity defined below. The ϑ-equation of motion becomes

$$\rho\bar\sigma^2\xi_\vartheta+\mathrm{i}\bar\sigma\frac{\rho\zeta}{r^2}\left[\left(1-\mu^2\right)\frac{\partial^2}{\partial\mu^2}\xi_\vartheta-4\mu\frac{\partial}{\partial\mu}\xi_\vartheta-\frac{5-2\mu^2}{1-\mu^2}\xi_\vartheta\right]$$

$$+\frac{\mathrm{i}\bar\sigma}{r^2}\frac{\partial}{\partial r}\left(\rho\zeta r^2\frac{\partial\xi_\vartheta}{\partial r}\right)+\left[2\mathrm{i}\rho\bar\sigma\Omega_\mathrm{s}\cos\vartheta\right]\xi_\varphi$$

$$-\left(\frac{P\chi_\rho}{r}\right)\frac{\partial}{\partial\vartheta}\left(\frac{\rho'}{\rho}\right)-\left(\frac{P\chi_T}{r}\right)\frac{\partial}{\partial\vartheta}\left(\frac{T'}{T}\right)$$

$$+\frac{P\chi_\mu}{r}\frac{\mathrm{d}\ln\mu_a}{\mathrm{d}r}\frac{\partial\xi_r}{\partial\vartheta}=-\frac{\rho}{r}\frac{\partial\Phi_\mathrm{T}}{\partial\vartheta}. \tag{9}$$

The φ-equation of motion can be expressed as

$$\rho\bar\sigma^2\xi_\varphi-\left[2\mathrm{i}\rho\bar\sigma\Omega_\mathrm{s}\sin\vartheta+\mathrm{i}m\frac{P\chi_\mu}{r\sin\vartheta}\frac{\mathrm{d}\ln\mu_a}{\mathrm{d}r}\right]\xi_r$$

$$-\left[2\mathrm{i}\rho\bar\sigma\Omega_\mathrm{s}\cos\vartheta\right]\xi_\vartheta+\left[\frac{\mathrm{i}mP\chi_\rho}{r\sin\vartheta}\right]\left(\frac{\rho'}{\rho}\right)$$

$$+\left[\frac{\mathrm{i}mP\chi_T}{r\sin\vartheta}\right]\left(\frac{T'}{T}\right)=\frac{\mathrm{i}m\rho}{r\sin\vartheta}\Phi_\mathrm{T}. \tag{10}$$

By applying the thermodynamic relation

$$\delta S=S'+\boldsymbol{\xi}\cdot\nabla S=\frac{P}{\rho T}\frac{1}{\Gamma_3-1}\left(\frac{\delta P}{P}-\Gamma_1\frac{\delta\rho}{\rho}\right)$$

where the symbol δ denotes a Lagrangian perturbation and Γ_j the adiabatic exponents of Chandrasekhar, the perturbed energy equation can be expressed as

$$\left[\frac{\mathrm{d}\ln P}{\mathrm{d}r}-\Gamma_1\frac{\mathrm{d}\ln\rho}{\mathrm{d}r}-\chi_\mu\frac{\mathrm{d}\ln\mu_a}{\mathrm{d}r}\right]\xi_r+\left[\chi_\rho-\Gamma_1\right]\left(\frac{\rho'}{\rho}\right)$$

$$+\left[\chi_T+\mathrm{i}\eta\left(\frac{m}{r\sin\vartheta}\right)^2\left(\frac{\mathrm{d}\ln T}{\mathrm{d}r}\right)^{-1}\right]\left(\frac{T'}{T}\right)$$

$$-\mathrm{i}\eta\left[\frac{1}{r^2}\frac{\partial}{\partial r}\left(r^2\frac{F_r'}{F}\right)+\frac{\mathrm{d}\ln F}{\mathrm{d}r}\left(\frac{F_r'}{F}\right)\right]$$

$$+\mathrm{i}\eta\left[\frac{\sin\vartheta}{r}\frac{\partial}{\partial\mu}\left(\frac{F_\vartheta'}{F}\right)-\frac{\cos\vartheta}{r\sin\vartheta}\left(\frac{F_\vartheta'}{F}\right)\right]=0 \tag{11}$$

where $\eta=(\Gamma_3-1)\frac{F}{\bar\sigma P}$ is a local characteristic radiative diffusion length in the star, with F the unperturbed (radial) energy flux. We have eliminated F_φ' with help of the φ-component of the radiative flux equation. In the stellar interior $\eta\simeq 0$ which corresponds to almost adiabatic response. However, even for 'high' frequencies $\bar\sigma/\Omega_\mathrm{c}\approx 1$ the diffusion length η becomes comparable to the scale height when the stellar surface is approached. The associated radiative energy losses give rise to damping of the tidally excited oscillations whereby the resulting phase lag with the companion generates a torque.

The perturbed radial radiative energy flux is given by

$$\left(\frac{F_r'}{F}\right)=\left(\frac{\mathrm{d}\ln T}{\mathrm{d}r}\right)^{-1}\frac{\partial}{\partial r}\left(\frac{T'}{T}\right)-\left(\kappa_T-4\right)\left(\frac{T'}{T}\right)$$

$$-\left(\kappa_\rho+1\right)\left(\frac{\rho'}{\rho}\right)+\kappa_X\frac{\partial\ln X}{\partial r}\xi_r \tag{12}$$

where $\kappa_\rho=\frac{\partial\ln\kappa}{\partial\ln\rho}$, $\kappa_T=\frac{\partial\ln\kappa}{\partial\ln T}$ and $\kappa_X=\frac{\partial\ln\kappa}{\partial\ln X}$, with X for the hydrogen abundance.

Finally the ϑ-component of the perturbed flux follows as

$$\left(\frac{F_\vartheta'}{F}\right)=\left(\frac{\mathrm{d}\ln T}{\mathrm{d}r}\right)^{-1}\frac{1}{r}\frac{\partial}{\partial\vartheta}\left(\frac{T'}{T}\right). \tag{13}$$

2.1. Boundary conditions

The differential equations are supplemented by the following boundary conditions: at the stellar centre we require ξ_r and F_r' to vanish, while at the stellar surface, we require the Lagrangian pressure perturbations to vanish

$$\frac{P'}{P}+\frac{\mathrm{d}\ln P}{\mathrm{d}r}\xi_r=0 \tag{14}$$

and the temperature and flux perturbations to fulfill Stefan–Boltzmann's law

$$\frac{F_r'}{F}=\left(\frac{2}{r}+4\frac{\mathrm{d}\ln T}{\mathrm{d}r}\right)\xi_r+4\left(\frac{T'}{T}\right). \tag{15}$$

Furthermore, ξ_ϑ and F_ϑ' must vanish on the rotation axis while in view of the symmetry of the tidal force we adopt mirror symmetry about the equatorial plane, i.e., for $\vartheta=\pi/2$ we also require ξ_ϑ and F_ϑ' to vanish.

2.2. The unperturbed stellar model

A recent version (Pols et al. 1995) of the stellar evolution code developed by Eggleton (1972) was used to construct the unperturbed stellar input model. The model represents a somewhat evolved main-sequence star of 10 $M_\odot$ with core hydrogen abundance of $X=0.4$ and $Z=0.02$. The mass in the convective core is approximately 2.1 $M_\odot$. The model comprises 1200 (radial) zones and was constructed with the OPAL opacities (Iglesias & Rogers 1996). The stellar radius equals $R_\mathrm{s}=3.825\times10^{11}$ cm, while the effective temperature $T_\mathrm{eff}=2.314\times10^4$ K and the stellar moment of inertia $I_\mathrm{s}=1.56\times10^{56}$ g cm^2. The break-up angular speed equals $\Omega_\mathrm{c}=1.54\times10^{-4}$ s^{-1}. The Brunt-Väisälä frequency $\mathcal{A}=\frac{1}{\rho}\frac{\mathrm{d}P}{\mathrm{d}r}\left(\frac{1}{\rho}\frac{\mathrm{d}\rho}{\mathrm{d}r}-\frac{1}{\Gamma_1 P}\frac{\mathrm{d}P}{\mathrm{d}r}\right)$ given in units of Ω_c, is plotted in Fig. 1. The Brunt-Väisälä frequency attains large values in the

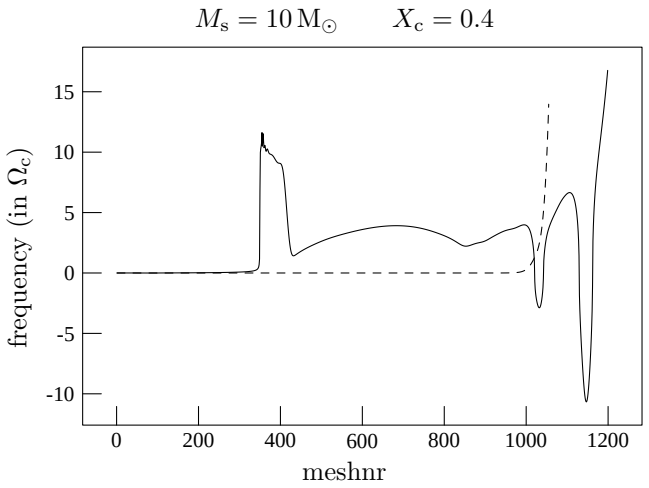

Fig. 1. Characteristics of the stellar model: continuous curve represents the Brunt-Väisälä frequency $\nu_{\rm BV} = {\rm sign}\mathcal{A}\sqrt{|\mathcal{A}|}$ in units of the stellar break-up speed$\Omega_{\rm c}$ as a function of radial mesh number. The dashed curve shows the forcing frequency $\bar{\sigma}$ for which the corresponding oscillation period equals the local thermal timescale.

region where the convective core has retreated during the evolution and a composition gradient is formed (the 'μ_a-gradient zone'). It can also be seen that there are two shallow convective shells near the stellar surface. The dashed curve shows the 'thermal frequency' $\nu_{\rm th} = 2\pi/\tau_{\rm th}$, where $\tau_{\rm th} = \frac{\rho\kappa(R_{\rm s}-r)^2\beta}{c(1-\beta)}$ is a local thermal timescale, κ is the opacity, c the velocity of light, and β the ratio of gas to total pressure. Non-adiabatic effects become important at locations where $\nu_{\rm th}$ is comparable or larger than the forcing frequency $\bar{\sigma}$. It can be seen in Fig. 1 that this is the case for the layers in and above the inner convective shell. At the inner edge of this shell $\nu_{\rm th} \simeq \Omega_{\rm c}$, at the outer edge $\nu_{\rm th} \simeq 5\Omega_{\rm c}$.

2.3. Turbulent viscosity in convective regions

In convective regions the equations of motion are supplemented by extra terms to account for the occurring turbulent dissipation, as described in PS97. For the coefficient of turbulent viscosity ζ we adopt a simple local mixing length approximation: $\zeta = \alpha\, H_p\, v_{\rm c}$, where H_p is the pressure scale height, $\alpha = 2$ is the mixing length parameter, and $v_{\rm c} = \left(\frac{F}{10\rho}\right)^{\frac{1}{3}}$ is a characteristic convective velocity. For high oscillation frequencies the viscosity is reduced (Goldreich & Keeley 1977) by a factor $\min\left(1, (\bar{\sigma}\tau_{\rm c})^{-2}\right)$, where $\tau_{\rm c} = \alpha H_p/v_{\rm c}$ is the convective timescale. We limit ζ to be everywhere less than 5×10^{12} cm^2 s^{-1}.

In the μ_a-gradient zone adjacent to the convective core, where the Brunt-Väisälä fequency attains large values, the tidal response has short wavelength and cannot be resolved on the grid when the forcing frequency $|\bar{\sigma}|$ drops to small values. We retain some viscosity in this region by letting the viscosity decay outwards from the boundary of the convective core (at $r_{\rm c}$) as $\zeta \propto \exp -[(r-r_{\rm c})/(0.1\,H_p)]^2$. Note in this respect that, although the composition gradient suppresses radial overshooting, horizontal turbulence may be well developed in this boundary layer between the core and envelope. Also the oscillation amplitudes are relatively large in this region.

3. The torque integral: transfer of energy and angular momentum

For a circular orbit the tidal potential (5) has no $m = 0$ component. However, since we wish to apply our results to eccentric binaries for which the tide has an axisymmetric time dependent component we replace the factor $e^{{\rm i}m(\omega t-\varphi)}$ by $e^{{\rm i}(\sigma t - m\varphi)}$ so that we can study $m = 0$ forcing. Once we have solved Eqs. 7–13 for a given stellar rotation rate $\Omega_{\rm s}$ and a given (l,m,σ), i.e. for a term

$$\Phi_{lm} = -f_{lm}\, r^l P_l^m(\cos\vartheta)\, \cos(\sigma t - \, m\varphi) \tag{16}$$

in the forcing potential (5), where $f_{lm} \propto M_{\rm p}/a^{l+1}$, the rate of angular momentum exchange with the companion's orbital motion can be calculated as an integral of the tidal force per unit volume $\boldsymbol{F}_{lm} = -\rho\nabla\Phi_{lm}$ over the volume of the star

$$\begin{aligned}\dot{H}_{\rm s} &= \int_\star \boldsymbol{r}\times\boldsymbol{F}_{lm}\,{\rm d}V \\ &= {\rm Re}\iiint -\frac{\partial\Phi_{lm}}{\partial\varphi}\rho'(r,\vartheta)\, r^2\,\sin\vartheta\,{\rm d}\vartheta\,{\rm d}\varphi\,{\rm d}r \\ &= m\pi f_{lm}\iint {\rm Im}(\rho')\, P_l^m(\cos\vartheta)\, r^{l+2}\sin\vartheta\,{\rm d}\vartheta\,{\rm d}r \\ &\equiv m\,\mathcal{T}_{lm}\end{aligned} \tag{17}$$

where Re and Im stand for the real and imaginary part. Since the torque and the stellar and orbital rotation vectors are all aligned, only the magnitude of the transferred spin and orbital angular momentum needs to be considered. The rate of tidal energy exchange with the (10 $M_\odot$) star can be expressed as

$$\begin{aligned}\dot{E}_{\rm s} &= \int_\star \boldsymbol{F}_{lm}\cdot\boldsymbol{v}\,{\rm d}V \\ &= -{\rm Re}\int_\star \rho_0\nabla\Phi_{lm}\cdot\boldsymbol{v}'\,{\rm d}V - {\rm Re}\int_\star \rho'\nabla\Phi_{lm}\cdot\boldsymbol{v}_{\rm rot}\,{\rm d}V.\end{aligned} \tag{18}$$

Substituting $\boldsymbol{v}' = {\rm i}\bar{\sigma}\boldsymbol{\xi}$ and $\boldsymbol{v}_{\rm rot} = \Omega_{\rm s} r\sin\vartheta\,\hat{\boldsymbol{e}}_\varphi$ we find, after taking the real part, that the second integral on the right hand side equals $m\Omega_{\rm s}\mathcal{T}_{lm}$. The first integral on the right hand side can be rewritten by applying the equation of continuity (7). Partial integration then shows that this term is also proportional to $\mathcal{T}_{lm}$ and equals $\bar{\sigma}\mathcal{T}_{lm}$. Concluding, we find for the tidally induced rate of respectively the energy and angular momentum change in the star:

$$\dot{E}_{\rm s} = \sigma\mathcal{T}_{lm} \tag{19}$$

$$\dot{H}_{\rm s} = m\mathcal{T}_{lm} \tag{20}$$

where the torque integral is given by

$$\mathcal{T}_{lm} = \pi f_{lm}\int_{-1}^{1}\int_0^{R_{\rm s}} {\rm Im}\left(\rho'(r,\mu)\right) P_l^m(\mu)\, r^{l+2}\,{\rm d}\mu\,{\rm d}r \tag{21}$$

with $\mu = \cos\vartheta$.

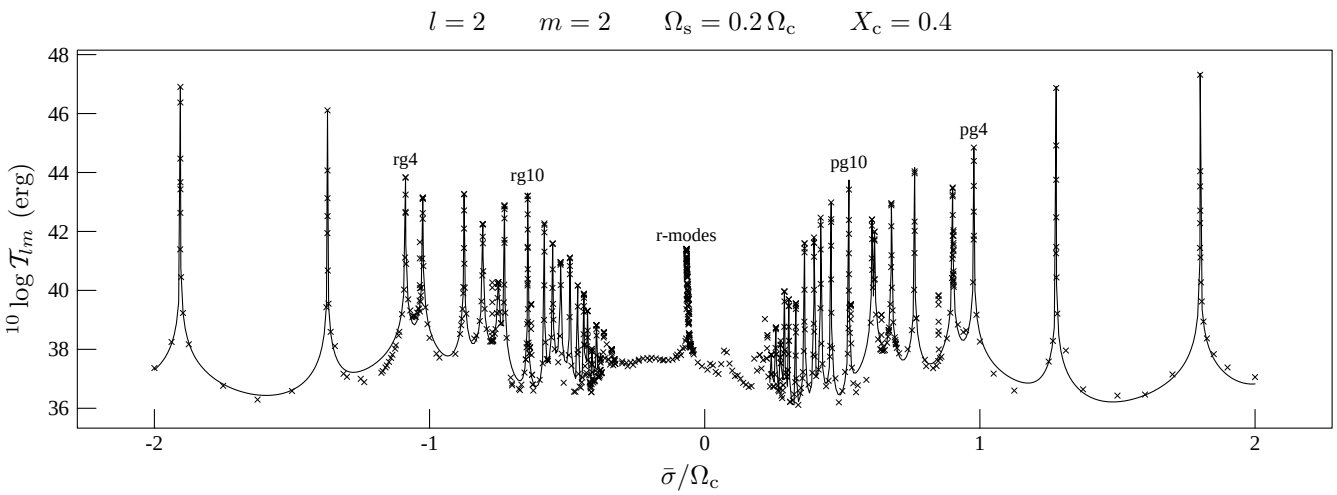

Fig. 2. Torque integral $\mathcal{T}_{lm}$ versus forcing frequency $\bar{\sigma}$ for forcing with $l = 2$ and $m = 2$ on a 10 $M_\odot$ star rotating at twenty percent of breakup speed. Prograde and retrograde $g^2_{\pm k}$-modes with $k = 4$ and 10 are labeled, as well as the location of the r-modes. Crosses denote calculated points, while the drawn continuous curve represents a fit, see text.

4. Numerical procedure

The set of partial differential Eqs. 7–13 with boundary conditions (14) and (15) is approximated by a set of finite difference equations (FDE's) on a 2D grid in r and ϑ, i.e. on a meridional plane through the star. The FDE's are similar (except for the extra terms associated with the μ_a-gradient) to those described in SP97 and are solved by the same implicit scheme as given in that paper. We use a grid of 1200 zones in the radial and 46 zones in the ϑ direction, analogous to the one used in SP97. Since the radial grid is staggered, with part of the unknown perturbations defined on the odd and the rest on the even zones, the effective number of radial zones is 600.

For given values of (l, m, σ) in the applied forcing potential (16) and for a given uniform rotation rate Ω_s of the star we can thus obtain the stellar response, i.e. the complex valued perturbations ξ_r, ξ_ϑ, ξ_φ, $\left(\frac{F'_r}{F}\right)$, $\left(\frac{F'_\vartheta}{F}\right)$, $\left(\frac{F'_\varphi}{F}\right)$ and $\left(\frac{\rho'}{\rho}\right)$, $\left(\frac{T'}{T}\right)$ on the 2D grid in the meridional plane of the perturbed star. By multiplying these values with the common factor $e^{i(\sigma t - m\varphi)}$ we obtain the non-adiabatic stellar response to the prescribed tidal forcing throughout the star.

Because the 2D implicit numerical scheme involves many (complex) matrix invertions the solution requires large computer facilities and it is essential to use an economic method for tracing the many resonances with the free stellar oscillation modes required to study the dynamical tide in a rotating star. The resonances are searched in frequency ($\bar{\sigma}$) space by by tracing the maximum of the function $\Psi(\bar{\sigma}) = \sum_{i,j} \boldsymbol{\xi}_{i,j} \cdot \boldsymbol{\xi}^*_{i,j}$ where $\boldsymbol{\xi}$ is the displacement vector, a $*$ denotes complex conjugation and i and j run over the radial and ϑ grid, respectively. The maxima of Ψ are searched by using a robust method based on cubic interpolation (NAG library routine) which requires the calculation of the first derivative $\frac{d\Psi}{d\bar{\sigma}} = \sum_{i,j} \left(\boldsymbol{\xi}_{i,j} \cdot \frac{\partial \boldsymbol{\xi}^*_{i,j}}{\partial \bar{\sigma}} + \boldsymbol{\xi}^*_{i,j} \cdot \frac{\partial \boldsymbol{\xi}_{i,j}}{\partial \bar{\sigma}} \right)$. Fortunately, the derivatives $\frac{\partial \boldsymbol{\xi}}{\partial \bar{\sigma}}$ and $\frac{\partial \boldsymbol{\xi}^*}{\partial \bar{\sigma}}$ can be obtained cheaply once we have obtained the solution of the perturbations $\boldsymbol{\xi}$, etc. For by differentiating Eqs. 7–13 with respect to $\bar{\sigma}$ we arrive at the same equations, except that the unknowns are now the derivatives of the perturbations (i.e. $\frac{\partial \boldsymbol{\xi}}{\partial \bar{\sigma}}$ instead of $\boldsymbol{\xi}$, etc.), while the right hand sides can be expressed in terms of the solved perturbations. The right hand side for equation (8) for example becomes $-2\rho\bar{\sigma}\xi_r - 2i\rho\Omega_s \sin\vartheta\, \xi_\varphi$. By storing the relevant inverted matrices during the solution procedure for the perturbations we then can simply combine the stored matrices with the adapted right hand sides to obtain a solution for $\frac{\partial \boldsymbol{\xi}}{\partial \bar{\sigma}}$ at almost no extra costs.

5. Results

From now on we will express all frequencies in units of $\Omega_c = 1.54 \times 10^{-4}$ s^{-1}. By varying the forcing frequency $\bar{\sigma} = \sigma - m\Omega_s$ (in the corotating frame) for the $l = 2$ terms in the forcing potential (16) and by calculating the stellar response, we can search for resonances with the free stellar oscillation modes, applying the procedure described in the previous section. We adopted various values for the rotation rate of the 10 $M_\odot$ star: $\Omega_s = 0$, 0.1, 0.2, 0.3 and 0.4.

We traced the resonances with g^2_k-modes (up to $k = 20$) for both prograde and retrograde g^2-modes. The lower index of g denotes k, the number of radial nodes in the displacement eigenvector, whereby the minus sign denotes a retrograde mode. Note that we characterize retrograde modes (i.e. modes that propagate in the direction counter to the stellar rotation) by negative values of the oscillation frequency $\bar{\sigma}$, i.e. we take $m > 0$ for both prograde and retrograde modes. For rotating stars there is in addition a compact spectrum of r-modes, for slightly negative frequencies. The $l = 2$ component of the tidal potential excites r-modes with a predominant $l = 3$ component. Note that because we consider binary systems in which both stars are aligned perpendicular to the orbital plane the ($l = 2$) forcing has only $m = 0$ and $|m| = 2$ components, i.e. $f_{21} = 0$.

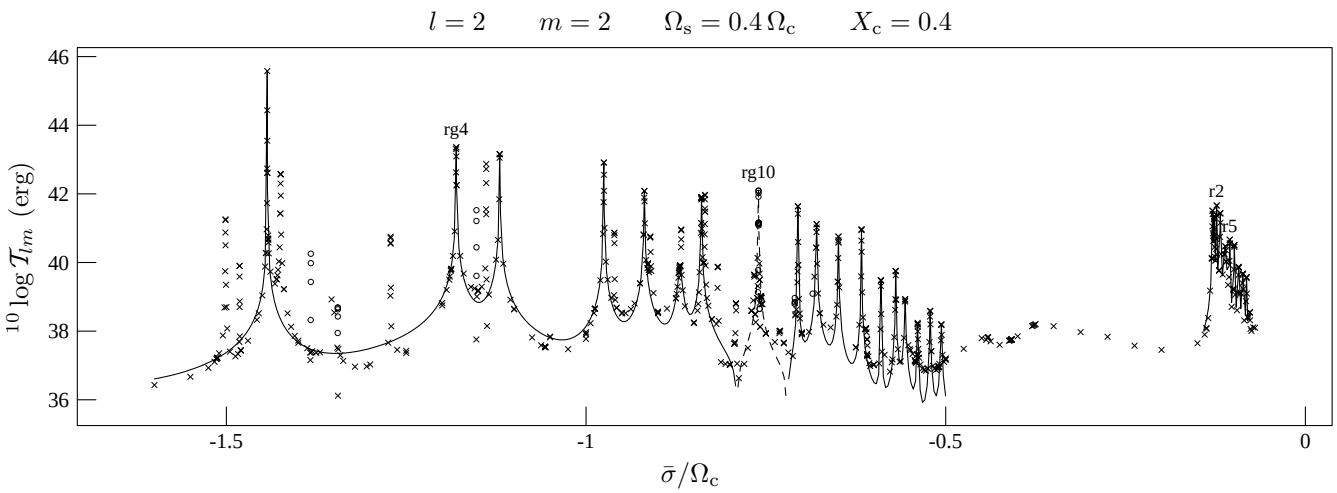

Fig. 3. Torque integral $\mathcal{T}_{lm}$ versus (retrograde) forcing frequency $\bar{\sigma}$ for forcing with $l = 2$ and $m = 2$ on a 10 $\mathrm{M}_\odot$ star rotating at fourty percent of breakup speed. Retrograde g^2_{-k}-modes with $k = 4$ and 10 (unstable) are labeled, as well as the r-modes with $k = 2$ and $k = 5$. Crosses and circles (unstable modes) denote calculated points. The peaks not fitted by the continuous curve correspond to resonances with higher spherical degrees $l = 4, 6, \ldots$

We can thus limit our calculations to either $|m| = 2$ or $m = 0$ resonances.

Note further that for all forcing frequencies $\bar{\sigma}$ we keep the factor f_{lm} in the forcing potential (16) constant by adopting a fixed value $a = 4R_\mathrm{s}$ and $M_\mathrm{p} = 1\mathrm{M}_\odot$. Because we solve the linearized problem all listed values for the tidal torque integral (21) can be simply scaled to the value for a required binary configuration by multiplying with a factor $(M_\mathrm{p}/\mathrm{M}_\odot)^2\,(4R_\mathrm{s}/a)^{2(l+1)}$, where a and M_p are the actual orbital separation and companion mass. Unless the companion is a compact star one should of course also take into account the (dynamical) tide in that star to determine the tidal evolution of the binary system.

5.1. Resonance fitting

Using the technique described in Sect. 4, we determine the resonances with g- and r-modes and evaluate the torque integral (21) from the calculated stellar response in the meridional plane of the 10 $\mathrm{M}_\odot$ star for all applied forcing frequencies. Close to each resonance we fit the obtained values for the torque integral by the resonance curve of a damped harmonic oscillator

$$\mathcal{T}_{lm}(\bar{\sigma}) = \frac{\mathcal{T}_{lm,0}}{\left(\frac{\bar{\sigma}^2 - \bar{\sigma}_0^2}{\bar{\sigma}_0 \Delta\bar{\sigma}}\right)^2 + 1} \tag{22}$$

with eigenfrequency $\bar{\sigma}_0$, resonance full width $\Delta\bar{\sigma}$ and peak value $\mathcal{T}_{lm,0}$. As a consequence of the Coriolis force, the stellar response to the $l = 2$ forcing contains a range of l-values (when we expand in spherical harmonics). However, we fit only the resonances with predominantly $l = 2$ (g-modes) or $l = 3$ (r-modes). In between $l = 2$ resonances we assume $\mathcal{T}_{lm}(\bar{\sigma})$ can be approximated by adding the contributions of the two adjacent $l = 2$ resonances. The detailed results of our numerical calculations are listed in Tables A1 to A4 in the appendix. Note that for a non-rotating star the $l = 2$ spectrum is degenerate in m, so that for $\Omega_\mathrm{s} = 0$ the resonance frequencies of $l = m = 2$ g-modes are given by Table A1.

It can be seen that, as expected, for $m = 0$ the g-mode resonance frequencies $\bar{\sigma}_0$ increase with Ω_s, as is true for $|\bar{\sigma}_0|$ for the retrograde $m = 2$ g-modes and the r-modes. However, the prograde $m = 2$ g-mode resonances shift to *lower* oscillation frequencies as Ω_s increases. Note in this respect that (approximate) conservation of radial vorticity, in combination with an increasing radial component of ambient rotation $\Omega_\mathrm{s} \cos\vartheta$ towards small colatitudes, tends to give retrograde wave propagation (see e.g. Unno et al. 1989).

5.2. Prograde and retrograde g-mode resonances

In Figs. 2 and 3 we show the tidal torque integral $\mathcal{T}_{lm}$ versus forcing frequency $\bar{\sigma}$ for a 10 $\mathrm{M}_\odot$ star rotating at a rate of 0.2 and 0.4, respectively. Crosses and open circles correspond to numerical results, while the continuous curve corresponds to the above mentioned fit to individual resonances. When the 10 $\mathrm{M}_\odot$ star rotates in the same sense as the orbital motion of its companion, the latter cannot excite modes with frequency (in the frame corotating with the star) less than $\bar{\sigma} = -m\Omega_\mathrm{s}$. Nevertheless, we have calculated the whole range $|\bar{\sigma}| \leq 2$. In Fig. 3, the circles and the dashed fit curve represent unstable modes for which the torque integral has a reversed sign compared to $\bar{\sigma}$ (see Sect. 5.4).

The prograde g-modes shift to substantially larger oscillation frequencies compared to the unevolved ZAMS stellar model of the same mass. The retrograde g-modes shift to more negative frequencies, so that for $\Omega_\mathrm{s} = 0.2$ no strong retrograde g-modes can be tidally excited, unless the rather unlikely case of retrograde stellar rotation applies. However, when the stellar rotation rate is increased more and more retrograde g-modes

are shifted into the 'tidal window': up to g^2_{-13} for $\Omega_s = 0.3$, and up to g^2_{-10} for $\Omega_s = 0.4$.

But note that when the binary is eccentric and the early type star's spin is approximately synchronized at periastron, strong (retrograde) r-modes can be tidally excited even for relatively low stellar rotation rates.

For small frequencies $|\bar{\sigma}|$ viscous damping in the μ_a-gradient zone becomes significant as the local wavelength of the response gets short and the adopted turbulent viscosity gets large due to the comparable timescale of 'convection' and oscillations (Sect. 2.3). Therefore the values for $\mathcal{T}_{lm}$ in the region between g^2_{-20} and the r-modes (and similarly for the corresponding positive frequency range) depend on the uncertain assumptions about the viscous dissipation. Switching off all viscous dissipation in the μ_a-gradient zone yields for $\Omega_s = 0.4$ in the frequency range $-0.4 < \bar{\sigma} < -0.2$ torque values about an order of magnitude smaller than shown in Fig. 3.

5.3. Effects of rapid rotation

Although centrifugal effects are no longer negligible for the high rotation rates ($\Omega_s = 0.4$) considered here the results are still of interest, even though centrifugal distortion is neglected, because they show the effect of strong coupling by the Coriolis force. Note in this respect that in the higher density interior regions the local break up speed is substantially larger than Ω_c. A full calculation with centrifugal distortion included would require a much larger computing effort.

The Coriolis force gives rise to strong coupling with modes of higher spherical degrees, so that for $l = 2$ forcing resonances with $l = 4, 6, 8, \ldots$ also become prominent, especially when located near a $l = 2$ resonance. Because the tidal forcing has $l = 2$ symmetry the latter resonances generally dominate, but all neighbouring resonances with $l > 2$ are also excited, so that the tidal response contains significant power over a broad range of (even) l-values. Often this makes mode identification (by means of a decomposition in Fourier-Legendre series of the eigenfunctions, see SP97) difficult since the power in different l-components are often comparable. One should consider the excited oscillation as a complex of coupled modes. Since, for a given frequency the g-modes with larger l have shorter wavelength, damping is enhanced, so that for large rotation rates the oscillation amplitude and the effective torque is reduced. This can be observed in Tables A1–A3, which show that the resonance area $\pi\Delta\bar{\sigma}\mathcal{T}_{lm}$ of the $l = 2$ g-modes initially increases with Ω_s but generally decreases when the rotation rate and inertial damping becomes large.

The indirectly excited higher l-resonances correspond to the peaks that have not been fitted in Fig. 3. This figure shows part of the retrograde oscillation spectrum for $\Omega_s = 0.4$. Most of the stable unfitted peaks between g^2_{-3} and g^2_{-5} correspond to what are (predominant) $l = 4$ resonances, except for the two nearest resonances around g^2_{-3}, which are identified as g^8_{-12} and g^{12}_{-18}. The unfitted peaks between g^2_{-6} and g^2_{-10} are all (predominant) $l = 4$ resonances, and can be identified as g^4_{-12} to g^4_{-18} consecutively. The g^2_{-8} and g^4_{-14} resonances can hardly be distinguished from each other, they lie so close together that they form a strongly coupled complex, whereby the g^4_{-14} resonance peaks one order of magnitude above the $l = 2$ resonance peak. Another symbiosis occurs for g^2_{-10} and g^4_{-18}, whereby, however, the former mode appears unstable and the latter stable. In this frequency range the resonances with $l > 4$ are heavily damped as they approach their asymptotic low frequency regime.

Table 1. Unstable $m = 2$ modes for $\Omega_s = 0.4$. The listed oscillation periods P_{in} are relative to the inertial frame, a minus sign denoting retrograde propagation.

mode	$\mathrm{Re}(\bar{\sigma})$	$\mathrm{Im}(\bar{\sigma})$	P_{in} (d)
g^8_{-12}	-1.3826	-1.1×10^{-5}	-0.81
g^{10}_{-17}	-1.3451	-5.3×10^{-5}	-0.87
g^6_{-13}	-1.1524	-1.2×10^{-5}	-1.34
g^2_{-10}	-0.7602	-1.2×10^{-4}	11.86
g^6_{14}	1.0580	-4.6×10^{-5}	0.25
g^6_{13}	1.1261	-4.3×10^{-5}	0.25
g^6_8	1.4610	-1.0×10^{-4}	0.21
g^8_8	2.1887	-2.4×10^{-5}	0.16

For still lower frequencies in the range around $\bar{\sigma} = -0.5$ the calculated response in between resonances is significantly stronger than the wings of the fitted $l = 2$ resonance curves due to the smeared out contributions of higher l components. At these frequencies the spectrum of $l = 4$ modes starts to become dense whereby radiative and viscous damping gets heavy due to the short wavelength of the response.

5.4. Unstable modes

It is now known (e.g. Dziembowski & Pamyatnykh 1993; Gautschy & Saio 1993) that most main sequence OB stars show unstable non-radial modes driven by the κ-mechanism associated with the metal opacity bump around 1.5×10^5 K in the OPAL opacity tables (Iglesias & Rogers 1996). Two necessary conditions for a mode to be unstable by the κ mechanism are that the Lagrangian pressure perturbation $\delta P/P$ must reach a maximum value (coming from the stellar centre) in the driving zone and that $2\pi/\bar{\sigma}$ is of order the thermal timescale in that region (e.g. Dziembowski et al. 1993). Obviously, when $|\bar{\sigma}| \ll \nu_{th} \equiv 2\pi/\tau_{th}$ in the ionization region that region is strongly non-adiabatic and no driving can occur. The 'thermal frequency' ν_{th} (Sect. 2.2) in the lower convective shell associated with the opacity bump varies between approximately 1 and 5.

When the stellar rotation rate is increased some inertially excited ($l > 2$) modes in our 10 $M_\odot$ model appear which have a torque integral $\mathcal{T}_{lm}$ with a sign opposite to that of $\bar{\sigma}$, which indicates instability. This can be checked by forcing the star with a complex frequency (Papaloizou et al. 1997) and searching for maximum amplitude in complex frequency space. It appears that the fundamental p^2_0 mode with $|\bar{\sigma}| \simeq 3.3$ is unstable for all rotation rates $\Omega_s = 0$ to 0.4. There are more unstable p-modes which we have not studied. Table 1 lists the unstable g-modes

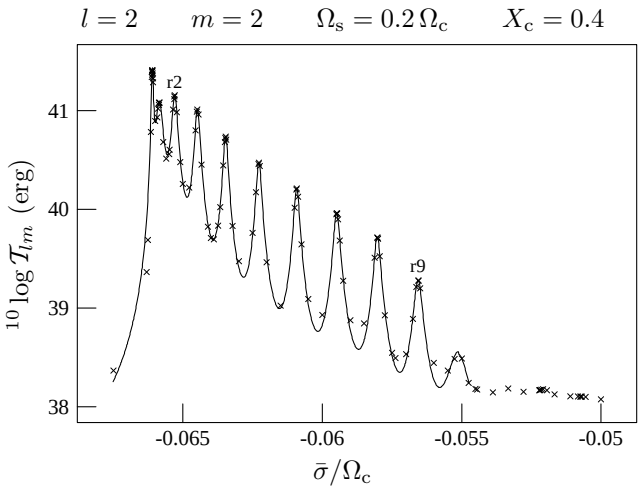

Fig. 4. Spectrum of r-modes: torque integral $\mathcal{T}_{lm}$ versus forcing frequency $\bar{\sigma}$ for forcing with $l = 2$ and $m = 2$ on a 10 $\mathrm{M}_\odot$ star rotating at twenty percent of breakup speed. Crosses denote calculated points, the drawn continuous curve represents a fit.

(prograde and retrograde) that are found for the highest rotation rate $\Omega_\mathrm{s} = 0.4$.

Only for the highest rotation rate ($\Omega_\mathrm{s} = 0.4$) an unstable $l = 2$ g-mode appears: the retrograde g^2_{-10} mode, with $\bar{\sigma} = -0.76$, which is located close to the stable g^4_{-18} resonance. The g^2_{-10} mode has rather low frequency for the κ-mechanism and is a bit peculiar in that it seems mixed with a strong short wavelength mode trapped in the μ_a gradient zone. The oscillation period (in inertial frame) of the unstable $l = 2$ mode happens to be quite long: about 12 days, while the adopted stellar rotation period is 1.2 days. We also find four unstable prograde g-modes, see Table 1. Our list of unstable modes is probably not exhaustive (except for $l = 2$), because we preferentially find those unstable modes which happen to be located near $l = 2$ resonances. Unstable modes, when excited by the tidal force, could give rise to tidal evolution counter to the normal direction of evolution.

5.5. r-modes

For small negative forcing frequencies around (e.g. Papaloizou & Pringle 1978): $\bar{\sigma} \simeq -\frac{2m\Omega_\mathrm{s}}{l(l+1)}$ strong resonances occur with quasi-toroidal oscillation modes analogous to Rossby modes in the earth's atmosfere (e.g. Pedlosky 1979). For these modes the fluid elements oscillate almost exclusively in the horizontal direction whereby the restoring force is provided by the Coriolis force (conservation of radial component of vorticity). Fig. 4 shows the variation of the torque integral $\mathcal{T}_{lm}$ as the forcing frequency runs through the r-mode region for a star rotating with $\Omega_\mathrm{s} = 0.2$. The adopted turbulent viscosity law in the μ_a gradient zone adjacent to the convective core causes the r-mode resonances to become rather broadened compared to the results for ZAMS models (SP97). When we switch off the viscosity in the μ_a-gradient zone the peak values for the torque become one or even two orders of magnitude higher, with a corresponding decrease of the resonance width. However, this will not make a large difference for the overall tidal evolution of the binary because the total area $\simeq \pi\Delta\bar{\sigma}\mathcal{T}_{lm,0}$ of each resonance remains approximately constant. The resonant interaction with r-modes gets stronger with increasing rotation rate Ω_s. This can be seen in Table A4 where the resonance area increases monotonically with Ω_s.

5.6. Excitation of inertial modes in the convective core

Similar to the results obtained in SP97 for a 20 $\mathrm{M}_\odot$ ZAMS star, we find inertial wave oscillations in the convective core and in the convective shell region when the forcing frequency falls in the inertial range $|\bar{\sigma}| < 2\Omega_\mathrm{s}$. When we artificially cut the radiative envelope from our stellar model we find a dense spectrum of modes in the core. For some frequencies the resonances in the core appear very strong. The general amplitudes are an order of magnitude larger (or more) compared to the full stellar model where the inertial waves can leak out of the core. This would suggest that the inertial modes could possibly excite gravity waves in the envelope (SP97). However, when we consider a model in which the convective core is cut away, we find in this frequency region values for the torque integral comparable to the ones calculated for the full stellar model. Therefore it seems the inertial core modes do not significantly contribute to the stellar torque in this somewhat evolved stellar model. However, the oscillations in the μ_a-gradient zone outside the convective core are poorly resolved for low frequencies, so that further studies with significantly more meshpoints in this region seem required to draw firm conclusions.

6. Conclusions

We have studied the linearized non-adiabatic tidal response of a somewhat evolved 10 $\mathrm{M}_\odot$ main sequence star to tidal forcing with spherical harmonics degree $l = 2$ and calculated the tidal exchange of energy and angular momentum with an orbiting companion as a function of stellar rotation rate taking the Coriolis force fully into account. We found, as expected, that with increasing rotation rate the inertial coupling with higher spherical degree oscillation modes gets stronger, so that when the rotation rate becomes comparable to or larger than the tidal oscillation frequency a significant amount of tidal energy is transferred to these higher degree oscillations. Because of enhanced damping of the higher l oscillations fast rotation reduces the resonant tidal interaction with $l = 2$ g-modes. However, this is compensated by the appearance of an additional spectrum of ($l > 2$) resonances that can be excited by the $l = 2$ tide.

With progressing nuclear evolution and consequent contraction of the stellar core the frequency of the g-mode oscillations increases, so that the 'gap' between potential resonances with strong retrograde g-modes and the strong r-modes widens. Thereby the retrograde strong g-modes disappear from the 'tidal window' ($\bar{\sigma}_\mathrm{res} > -m\Omega_\mathrm{s}$) so that spin-down of fast spinning early type binary stars depends on excitation of strongly

damped high radial order g-modes. This seems a not very efficient mechanism unless viscous effects (e.g. in the μ_a-gradient zone outside the convective core) are significant or perhaps driving by inertial resonances in the convective core occurs. But, when in an eccentric binary system, the early type star is nearly corotating at periastron r-mode resonances are very efficient in spinning the star further down to (pseudo)corotation. We expect a balance between spin-down by r-modes and spin-up by prograde g-modes excited by the high frequency components of the tidal forces near periastron. We intend to study this in a following paper, using the torque values determined here.

Acknowledgements. This work was sponsored by the Stichting Nationale Computerfaciliteiten (National Computing Facilities Foundation, NCF) for the use of supercomputing facilities, with financial support from the Netherlands Organization for Scientific Research (NWO).

References

Berthomieu G., Gonczi G., Graff P., Provost J., Rocca A., 1978, A&A 70, 597
Cowling T. G., 1941, MNRAS 101, 367
Dziembowski W. A., Pamyatnykh A., 1993, MNRAS 262, 204
Dziembowski W. A., Moskalik P., Pamyatnykh A., 1993, MNRAS 265, 588
Eggleton P. P., 1972, MNRAS 156, 361
Gautschy A., Saio H., 1993, MNRAS 262, 213
Goldreich P., Keeley D. A., 1977, ApJ 211, 934
Iglesias C. A., Rogers F. J., 1996, ApJ 464, 943
Kumar P., Goodman J., 1996, ApJ 466, 946
Lai D., 1997, ApJ 490, 847
Ledoux P., Walraven T., 1958, Handbuch der Physik, Springer Verlag
Morse P. M., Feshbach H., 1952, Methods of Theoretical Physics, Vol. II, McGraw Hill Book Comp.
Papaloizou J. C. B., Pringle J. E., 1978, MNRAS 182, 423
Papaloizou J. C. B., Savonije G. J., 1997, MNRAS 291, 651
Papaloizou J. C. B., Alberts F., Pringle J., Savonije G. J., 1997, MNRAS 284, 821
Pedlosky J., 1979, Geophysical fluid dynamics, Springer Verlag
Pols O. R., Tout C. A., Eggleton P. P., Han Z., 1995, MNRAS 274, 964
Savonije G. J., Papaloizou J. C. B., 1984, MNRAS 207, 685
Savonije G. J., Papaloizou J. C. B., 1997, MNRAS 291, 633
Unno W., Osaki Y., Ando H., Saio H., Shibahashi H., 1989, Nonradial oscillations of stars, Univ. of Tokyo Press
Zahn J., 1977, A&A 57, 383

Appendix A: Tables

Table A1. Fitting parameters for g_k^2-mode resonances with an $l = 2$, $m = 0$ tidal potential in a 10 $\mathrm{M}_\odot$ star with $X_c = 0.4$. All tabulated values for the torque integral have been obtained for a fixed orbital separation.

	$\Omega_\mathrm{s} = 0.0\,\Omega_\mathrm{c}$			$\Omega_\mathrm{s} = 0.2\,\Omega_\mathrm{c}$			$\Omega_\mathrm{s} = 0.4\,\Omega_\mathrm{c}$		
k	$\bar{\sigma}_0/\Omega_\mathrm{c}$	$\mathcal{T}_{lm,0}$ (erg)	$\Delta\bar{\sigma}/\Omega_\mathrm{c}$	$\bar{\sigma}_0/\Omega_\mathrm{c}$	$\mathcal{T}_{lm,0}$ (erg)	$\Delta\bar{\sigma}/\Omega_\mathrm{c}$	$\bar{\sigma}_0/\Omega_\mathrm{c}$	$\mathcal{T}_{lm,0}$ (erg)	$\Delta\bar{\sigma}/\Omega_\mathrm{c}$
1	2.2186	2.94×10^{45}	1.33×10^{-5}	2.2344	2.95×10^{45}	1.32×10^{-5}	2.2804	3.08×10^{45}	1.28×10^{-5}
2	1.8489	3.35×10^{45}	1.34×10^{-5}	1.8676	2.72×10^{45}	1.64×10^{-5}	1.9214	3.19×10^{45}	1.38×10^{-5}
3	1.3162	9.00×10^{44}	1.18×10^{-5}	1.3427	8.06×10^{44}	1.39×10^{-5}	1.4196	7.38×10^{43}	1.01×10^{-4}
4	1.0203	9.28×10^{42}	2.70×10^{-4}	1.0538	6.81×10^{42}	3.63×10^{-4}	1.1465	9.75×10^{42}	1.87×10^{-4}
5	0.9510	5.08×10^{41}	1.37×10^{-3}	0.9862	5.30×10^{41}	1.22×10^{-3}	1.0806	6.14×10^{41}	1.05×10^{-3}
6	0.8037	1.42×10^{42}	4.12×10^{-4}	0.8454	1.46×10^{42}	3.89×10^{-4}	0.9532	1.76×10^{42}	3.03×10^{-4}
7	0.7258	9.82×10^{40}	1.64×10^{-3}	0.7711	1.04×10^{41}	1.44×10^{-3}	0.8852	1.04×10^{41}	1.15×10^{-3}
8	0.6637	2.74×10^{39}	1.03×10^{-2}	0.7119	3.09×10^{39}	8.43×10^{-3}	0.8338	1.26×10^{40}	1.68×10^{-3}
9	0.6503	2.07×10^{41}	7.00×10^{-4}	0.7006	1.73×10^{41}	7.90×10^{-4}	0.8217	1.85×10^{41}	5.76×10^{-4}
10	0.5628	1.62×10^{42}	5.22×10^{-5}	0.6198	1.57×10^{42}	4.88×10^{-5}	0.7519	2.41×10^{41}	2.49×10^{-4}
11	0.4976	1.86×10^{41}	1.46×10^{-4}	0.5608	2.09×10^{41}	1.16×10^{-4}	0.6988	2.93×10^{40}	6.63×10^{-4}
12	0.4619	2.72×10^{40}	6.96×10^{-4}	0.5286	3.20×10^{40}	5.07×10^{-4}	0.6693	1.98×10^{40}	4.92×10^{-4}
13	0.4345	2.43×10^{40}	2.85×10^{-4}	0.5048	2.11×10^{40}	2.58×10^{-4}	0.6471	5.06×10^{39}	4.43×10^{-4}
14	0.3983	3.18×10^{40}	1.76×10^{-4}	0.4734	2.58×10^{40}	1.70×10^{-4}	0.6183	7.39×10^{39}	2.33×10^{-4}
15	0.3662	8.01×10^{38}	2.84×10^{-4}	0.4459	6.71×10^{38}	2.04×10^{-4}	0.5917	1.99×10^{37}	3.38×10^{-4}
16	0.3404	4.29×10^{38}	8.72×10^{-4}	0.4240	4.78×10^{38}	5.53×10^{-4}	0.5700	2.14×10^{38}	4.55×10^{-4}
17	0.3248	2.05×10^{38}	2.04×10^{-3}	0.4109	2.79×10^{38}	1.21×10^{-3}	0.5561	2.22×10^{38}	9.41×10^{-4}
18	0.3086	1.02×10^{37}	1.60×10^{-3}	0.3977	1.45×10^{37}	1.00×10^{-3}	0.5422	2.87×10^{37}	1.34×10^{-3}
19	0.2904	8.10×10^{37}	1.47×10^{-3}	0.3827	9.18×10^{37}	9.17×10^{-4}	0.5262	3.99×10^{37}	7.42×10^{-4}
20	0.2734	5.86×10^{36}	2.82×10^{-3}	0.3689	1.05×10^{37}	1.95×10^{-3}	0.5105	2.24×10^{37}	1.04×10^{-3}

Table A2. Fitting parameters for *retrograde* g_k^2-mode resonances with an $l = 2$, $m = 2$ tidal potential in a 10 $\mathrm{M}_\odot$ star with $X_c = 0.4$. All tabulated values for the torque integral have been obtained for a fixed orbital separation.

	$\Omega_\mathrm{s} = 0.2\,\Omega_\mathrm{c}$			$\Omega_\mathrm{s} = 0.3\,\Omega_\mathrm{c}$			$\Omega_\mathrm{s} = 0.4\,\Omega_\mathrm{c}$		
k	$\bar{\sigma}_0/\Omega_\mathrm{c}$	$\mathcal{T}_{lm,0}$ (erg)	$\Delta\bar{\sigma}/\Omega_\mathrm{c}$	$\bar{\sigma}_0/\Omega_\mathrm{c}$	$\mathcal{T}_{lm,0}$ (erg)	$\Delta\bar{\sigma}/\Omega_\mathrm{c}$	$\bar{\sigma}_0/\Omega_\mathrm{c}$	$\mathcal{T}_{lm,0}$ (erg)	$\Delta\bar{\sigma}/\Omega_\mathrm{c}$
1	-2.2734	-5.59×10^{46}	3.00×10^{-6}	-2.3042	-4.05×10^{46}	3.39×10^{-6}	-2.3376	-2.91×10^{46}	3.82×10^{-6}
2	-1.9055	-8.22×10^{46}	2.75×10^{-6}	-1.9368	-6.93×10^{46}	2.77×10^{-6}	-1.9700	-5.54×10^{46}	3.05×10^{-6}
3	-1.3709	-1.29×10^{46}	3.80×10^{-6}	-1.4047	-9.02×10^{45}	4.58×10^{-6}	-1.4431	-3.86×10^{45}	8.73×10^{-6}
4	-1.0872	-6.92×10^{43}	1.41×10^{-4}	-1.1306	-3.91×10^{43}	1.95×10^{-4}	-1.1804	-2.28×10^{43}	2.54×10^{-4}
5	-1.0246	-1.42×10^{43}	2.97×10^{-4}	-1.0697	-1.41×10^{43}	2.77×10^{-4}	-1.1200	-1.45×10^{43}	2.70×10^{-4}
6	-0.8745	-1.88×10^{43}	1.31×10^{-4}	-0.9216	-1.28×10^{43}	1.56×10^{-4}	-0.9752	-8.23×10^{42}	1.89×10^{-4}
7	-0.8064	-1.79×10^{42}	4.57×10^{-4}	-0.8592	-1.40×10^{42}	5.35×10^{-4}	-0.9189	-1.22×10^{42}	4.96×10^{-4}
8	-0.7501	-1.93×10^{40}	3.07×10^{-3}	-0.8065	-1.17×10^{40}	3.51×10^{-3}	-0.8693	-8.35×10^{39}	3.84×10^{-3}
9	-0.7277	-7.76×10^{42}	9.15×10^{-5}	-0.7794	-7.71×10^{42}	7.48×10^{-5}	-0.8395	-7.92×10^{41}	4.30×10^{-4}
10	-0.6434	-2.01×10^{43}	1.92×10^{-5}	-0.6985	-9.26×10^{42}	3.33×10^{-5}	-0.7602	1.27×10^{42}	1.97×10^{-4}
11	-0.5827	-1.88×10^{42}	5.97×10^{-5}	-0.6417	-7.80×10^{41}	1.05×10^{-4}	-0.7054	-4.40×10^{41}	1.25×10^{-4}
12	-0.5525	-3.89×10^{41}	2.51×10^{-4}	-0.6143	-3.04×10^{41}	2.75×10^{-4}	-0.6795	-1.30×10^{41}	4.90×10^{-4}
13	-0.5238	-8.97×10^{40}	5.71×10^{-4}	-0.5849	-2.58×10^{41}	1.31×10^{-4}	-0.6491	-5.72×10^{40}	4.04×10^{-4}
14	-0.4899	-1.29×10^{41}	2.63×10^{-4}	-0.5525	-1.73×10^{41}	1.60×10^{-4}	-0.6170	-9.25×10^{40}	1.90×10^{-4}
15	-0.4612	-1.47×10^{40}	1.44×10^{-4}	-0.5253	-6.51×10^{39}	2.64×10^{-4}	-0.5900	-3.05×10^{39}	2.33×10^{-4}
16	-0.4390	-7.70×10^{39}	4.13×10^{-4}	-0.5046	-6.79×10^{39}	4.52×10^{-4}	-0.5695	-5.67×10^{39}	4.15×10^{-4}
17	-0.4259	-2.04×10^{39}	6.86×10^{-4}	-0.4919	-1.24×10^{39}	8.12×10^{-4}	-0.5564	-8.61×10^{38}	9.36×10^{-4}
18	-0.4101	-1.02×10^{38}	6.33×10^{-4}	-0.4757	-1.15×10^{38}	8.91×10^{-4}	-0.5391	-1.80×10^{38}	6.93×10^{-4}
19	-0.3935	-6.68×10^{38}	9.02×10^{-4}	-0.4592	-6.61×10^{38}	6.68×10^{-4}	-0.5216	-3.90×10^{38}	6.60×10^{-4}
20	-0.3787	-4.97×10^{37}	2.03×10^{-3}	-0.4445	-7.44×10^{37}	1.29×10^{-3}	-0.5060	-1.57×10^{38}	9.52×10^{-4}

Table A3. Fitting parameters for *prograde* g_k^2-mode resonances with an $l = 2$, $m = 2$ tidal potential in a 10 $\mathrm{M}_\odot$ star with $X_c = 0.4$. All tabulated values for the torque integral have been obtained for a fixed orbital separation.

	$\Omega_\mathrm{s} = 0.2\,\Omega_\mathrm{c}$			$\Omega_\mathrm{s} = 0.3\,\Omega_\mathrm{c}$			$\Omega_\mathrm{s} = 0.4\,\Omega_\mathrm{c}$		
k	$\bar{\sigma}_0/\Omega_\mathrm{c}$	$\mathcal{T}_{lm,0}$ (erg)	$\Delta\bar{\sigma}/\Omega_\mathrm{c}$	$\bar{\sigma}_0/\Omega_\mathrm{c}$	$\mathcal{T}_{lm,0}$ (erg)	$\Delta\bar{\sigma}/\Omega_\mathrm{c}$	$\bar{\sigma}_0/\Omega_\mathrm{c}$	$\mathcal{T}_{lm,0}$ (erg)	$\Delta\bar{\sigma}/\Omega_\mathrm{c}$
1	2.1724	1.92×10^{47}	1.55×10^{-6}	2.1519	2.38×10^{47}	1.43×10^{-6}	2.1330	2.98×10^{47}	1.26×10^{-6}
2	1.8006	2.31×10^{47}	1.39×10^{-6}	1.7781	1.49×10^{47}	3.53×10^{-6}	1.7587	6.71×10^{46}	5.67×10^{-6}
3	1.2773	8.31×10^{46}	1.11×10^{-6}	1.2623	6.55×10^{46}	1.61×10^{-6}	1.2498	5.15×10^{45}	2.28×10^{-5}
4	0.9780	7.33×10^{44}	2.94×10^{-5}	0.9638	1.37×10^{45}	1.87×10^{-5}	0.9532	2.65×10^{45}	1.13×10^{-5}
5	0.9011	3.11×10^{43}	1.33×10^{-4}	0.8836	3.26×10^{43}	1.23×10^{-4}	0.8692	6.30×10^{43}	7.10×10^{-5}
6	0.7629	1.46×10^{44}	3.29×10^{-5}	0.7508	2.57×10^{44}	2.17×10^{-5}	0.7425	2.56×10^{44}	2.56×10^{-5}
7	0.6783	9.16×10^{42}	1.27×10^{-4}	0.6637	1.61×10^{43}	8.03×10^{-5}	0.6534	2.18×10^{43}	6.48×10^{-5}
8	0.6171	1.00×10^{42}	5.41×10^{-4}	0.6044	3.29×10^{42}	2.64×10^{-4}	0.5959	6.81×10^{42}	1.62×10^{-4}
9	0.6078	2.55×10^{42}	2.76×10^{-4}	0.5948	1.66×10^{42}	2.75×10^{-4}	0.5853	7.28×10^{41}	3.55×10^{-4}
10	0.5242	5.54×10^{43}	1.11×10^{-5}	0.5152	3.09×10^{43}	2.21×10^{-5}	0.5103	1.05×10^{43}	7.07×10^{-5}
11	0.4596	9.80×10^{42}	2.08×10^{-5}	0.4517	3.54×10^{42}	6.27×10^{-5}	0.4476	4.44×10^{42}	5.33×10^{-5}
12	0.4213	2.92×10^{42}	4.04×10^{-5}	0.4125	5.07×10^{42}	2.35×10^{-5}	0.4077	6.97×10^{42}	1.70×10^{-5}
13	0.3971	6.25×10^{41}	5.02×10^{-5}	0.3896	2.15×10^{41}	1.19×10^{-4}	0.3855	2.86×10^{41}	6.81×10^{-5}
14	0.3627	4.18×10^{41}	6.77×10^{-5}	0.3565	2.87×10^{41}	8.87×10^{-5}	0.3536	1.76×10^{41}	1.30×10^{-4}
15	0.3313	3.67×10^{39}	1.56×10^{-4}	0.3256	1.99×10^{39}	1.69×10^{-4}	0.3232	1.54×10^{39}	1.24×10^{-4}
16	0.3057	5.00×10^{39}	2.52×10^{-4}	0.3004	3.85×10^{39}	2.43×10^{-4}	0.2981	3.26×10^{39}	2.33×10^{-4}
17	0.2896	9.20×10^{39}	2.98×10^{-4}	0.2840	9.48×10^{39}	2.83×10^{-4}	0.2813	9.43×10^{39}	2.65×10^{-4}
18	0.2758	2.06×10^{38}	6.43×10^{-4}	0.2711	3.34×10^{38}	6.40×10^{-4}	0.2690	6.06×10^{38}	5.35×10^{-4}
19	0.2586	5.45×10^{38}	1.08×10^{-3}	0.2545	5.09×10^{38}	1.01×10^{-3}	0.2529	4.88×10^{38}	9.27×10^{-4}
20	0.2421	6.70×10^{37}	1.66×10^{-3}	0.2384	8.80×10^{37}	1.47×10^{-3}	0.2370	1.05×10^{38}	1.28×10^{-3}

Table A4. Fitting parameters for r_k^3-mode resonances with an $l = 2$, $m = 2$ tidal potential in a 10 $\mathrm{M}_\odot$ star with $X_c = 0.4$. All tabulated values for the torque integral have been obtained for a fixed orbital separation.

	$\Omega_\mathrm{s} = 0.1\,\Omega_\mathrm{c}$			$\Omega_\mathrm{s} = 0.2\,\Omega_\mathrm{c}$		
k	$\bar{\sigma}_0/\Omega_\mathrm{c}$	$\mathcal{T}_{lm,0}$ (erg)	$\Delta\bar{\sigma}/\Omega_\mathrm{c}$	$\bar{\sigma}_0/\Omega_\mathrm{c}$	$\mathcal{T}_{lm,0}$ (erg)	$\Delta\bar{\sigma}/\Omega_\mathrm{c}$
0	-3.3237×10^{-2}	-5.63×10^{41}	5.71×10^{-6}	-6.6098×10^{-2}	-2.57×10^{41}	7.35×10^{-5}
1	-3.3191×10^{-2}	-7.69×10^{40}	4.80×10^{-5}	-6.5845×10^{-2}	-1.20×10^{41}	2.40×10^{-4}
2	-3.3133×10^{-2}	-1.04×10^{41}	3.61×10^{-5}	-6.5292×10^{-2}	-1.41×10^{41}	2.03×10^{-4}
3	-3.3031×10^{-2}	-8.46×10^{40}	3.03×10^{-5}	-6.4479×10^{-2}	-1.03×10^{41}	1.87×10^{-4}
4	-3.2896×10^{-2}	-4.67×10^{40}	3.14×10^{-5}	-6.3467×10^{-2}	-5.42×10^{40}	1.85×10^{-4}
5	-3.2730×10^{-2}	-2.43×10^{40}	3.46×10^{-5}	-6.2277×10^{-2}	-2.96×10^{40}	2.00×10^{-4}
6	-3.2534×10^{-2}	-1.27×10^{40}	3.97×10^{-5}	-6.0922×10^{-2}	-1.62×10^{40}	2.11×10^{-4}
7	-3.2315×10^{-2}	-7.93×10^{39}	4.26×10^{-5}	-5.9485×10^{-2}	-9.14×10^{39}	2.38×10^{-4}
8	-3.2084×10^{-2}	-4.02×10^{39}	4.63×10^{-5}	-5.8029×10^{-2}	-5.19×10^{39}	2.51×10^{-4}
9	-3.1842×10^{-2}	-1.48×10^{39}	5.51×10^{-5}	-5.6565×10^{-2}	-1.89×10^{39}	3.12×10^{-4}
10	-3.1581×10^{-2}	-2.24×10^{38}	8.18×10^{-5}	-5.5121×10^{-2}	-3.39×10^{38}	7.66×10^{-4}
	$\Omega_\mathrm{s} = 0.3\,\Omega_\mathrm{c}$			$\Omega_\mathrm{s} = 0.4\,\Omega_\mathrm{c}$		
k	$\bar{\sigma}_0/\Omega_\mathrm{c}$	$\mathcal{T}_{lm,0}$ (erg)	$\Delta\bar{\sigma}/\Omega_\mathrm{c}$	$\bar{\sigma}_0/\Omega_\mathrm{c}$	$\mathcal{T}_{lm,0}$ (erg)	$\Delta\bar{\sigma}/\Omega_\mathrm{c}$
0	-9.8117×10^{-2}	-1.74×10^{41}	3.87×10^{-4}	-1.2898×10^{-1}	-3.26×10^{41}	4.25×10^{-4}
1	-9.7284×10^{-2}	-1.12×10^{41}	9.12×10^{-4}	-1.2685×10^{-1}	-2.23×10^{41}	6.54×10^{-4}
2	-9.5530×10^{-2}	-1.95×10^{41}	3.78×10^{-4}	-1.2328×10^{-1}	-4.60×10^{41}	3.18×10^{-4}
3	-9.3144×10^{-2}	-1.51×10^{41}	3.93×10^{-4}	-1.1833×10^{-1}	-2.73×10^{41}	4.26×10^{-4}
4	-9.0057×10^{-2}	-4.14×10^{40}	7.76×10^{-4}	-1.1145×10^{-1}	-3.08×10^{40}	2.42×10^{-3}
5	-8.6610×10^{-2}	-2.93×10^{40}	4.95×10^{-4}	-1.0515×10^{-1}	-4.60×10^{40}	5.49×10^{-4}
6	-8.2982×10^{-2}	-2.23×10^{40}	4.14×10^{-4}	-9.8842×10^{-2}	-3.21×10^{40}	5.26×10^{-4}
7	-7.9327×10^{-2}	-9.10×10^{39}	5.65×10^{-4}	-9.2639×10^{-2}	-7.71×10^{39}	1.12×10^{-3}
8	-7.5855×10^{-2}	-5.14×10^{39}	6.24×10^{-4}	-8.6945×10^{-2}	-5.05×10^{39}	1.08×10^{-3}
9	-7.2437×10^{-2}	-2.03×10^{39}	7.43×10^{-4}	-8.1781×10^{-2}	-3.74×10^{39}	7.49×10^{-4}
10	-6.9712×10^{-2}	-2.28×10^{38}	3.98×10^{-3}	-7.7343×10^{-2}	-3.83×10^{38}	1.02×10^{-3}